Caving 2026 – A van As, D Cumming-Potvin & J Wesseloo (eds)

doi:10.36487/ACG_repo/2645_61

A study of seismic tomography for cave shape model estimation

Septian Prahastudhi [a,*], Roy William [a], Erin Bailey [b], Willem de Beer [c]

[a] *ESG Solutions, Indonesia*

[b] *ESG Solutions, Canada*

[c] *ESG Solutions, Australia*

Abstract

In block caving operations, knowing the shape and the evolution of the cave is critical since these factors influence local and regional ground stability, and impact operational strategy. While open hole logging using a borehole camera is one of the most accurate methods for delineating the cave shape, drilling near the cave is challenging and largely impractical due to operational, economic and physical constraints. Operators therefore need indirect methods such as subsurface imaging. In seismology, passive tomography has several applications: it is used in studying the Earth's structure, in mining, in the geothermal energy industry and in hydrocarbons extraction. Passive tomography uses seismic waves recorded by seismic arrays. A key advantage is that tomography is not dependent on the number of events, but instead relies on the relative distribution of sensors and events and on the density of ray paths. Tomographic inversion requires an initial velocity model. In applications which aim to track stress evolution around large voids, this seed model is usually a 3D (heterogeneous) velocity model derived from the estimated cave shape. This cave shape is informed by limited open hole measurements and/or height of draw (HOD) estimates that are subject to biases introduced by, for example, the flow model assumed. The use of such a model can lead to the inversion result being driven excessively by the 3D velocity model rather than by actual cave growth. In this study, we investigate time lapse passive tomography imaging in two different producing block caving mines and compare the results obtained with and without the seed 3D velocity model. This allows an assessment of the dependence of results on a priori assumptions and allows for comparison with open hole and HOD estimates.

Keywords: *seismic tomography, cave shape, velocity model, ray path, height of draw*

1 Introduction

Understanding the cave geometry and how it evolves during the mining process is very important. The operational risk associated with block caving must be monitored with the use of instrumentation to ensure safety of personnel and underground infrastructure (Dawn 2019). Direct measurements such as borehole cameras, cave tracker systems and smart markers can provide a better understanding of cave delineation. However, these methods are often high cost and sometimes challenging from an operational perspective as it is almost impossible to drill boreholes in all directions throughout the cave, leading to poor resolution of the cave growth. For this reason, methods that allow indirect subsurface imaging will be beneficial.

Passive velocity tomography has been widely used. In crustal seismology, Muttaqy et al. (2022) use tomography to image the lithospheric structure beneath central Java Indonesia which relation with the earthquake. Grand et al. (1997) also used tomography to capture the seismic velocity beneath the Earth. In another example, Rahman et al. (2013) use passive seismic tomography to minimise subsurface

* Corresponding author. Email address: septian.prahastudhi@esgsolutions.com

uncertainties in oil and gas exploration (2013); using seismic waves recorded by sensors around the cave, the internal velocity of the rock mass can be reconstructed where the wave propagates. An advantage of seismic tomography is that it yields information about seismically inactive regions of the rock mass if there are source-sensor ray paths travelling through these regions. Areas of increasing stress show increasing seismic velocities since increased stress will result in the closing of joints, fractures, microcracks and pore space, all leading to an overall increasing stiffness of the rock. Decreasing seismic velocity can be interpreted as areas of stress relaxation/destressing and can also indicate areas of damaged rock (inelastic deformation) or post-peak rock failure (Kamp et al. 2022).

Several studies have applied tomography in block caving environments. Melati et al. (2025) combine tomography with numerical modelling to monitor cave propagation. Afrouz & Westman (2018) use tomography to identify high velocities in the abutment and above the cave crown, while Setiadi et al. (2015) use tomography based on a Fresnel zone to predict the fracture positions around a cave. de Beer et al. (2024) integrate tomographic results with stress inversion to monitor the cave stress evolution around the cave. However, these studies all use a 3D velocity model which is built from an assumed cave shape as a starting estimate. Another study by Kamp et al. (2022) presents a case where the tomography results are integrated with a numerical a model to evaluate the likely cave shape.

In this study, tomographic inversion was performed using a 3D velocity model and a 1D velocity model as the starting velocity assumption for two different block cave sites. The 3D velocity model is based on the estimated cave shape derived from available direct measurements such as borehole cameras, beacons, smart markers and mucking (HOD). The inversion results may be affected by the uncertainties of the estimated cave geometry that is incorporated in the 3D velocity model, potentially introducing bias in the interpretation. This study investigates this using time lapse tomography in two different producing block caving mines, comparing results obtained with a 1D velocity model and a 3D velocity model to assess the influence of prior velocity model assumptions. The results will be compared to independent observations for consistency.

2 Velocity model

In block caving, event source location is often more accurately determined using a 3D velocity model. Collins et al. (2014) compared the accuracy between a 3D and a 1D velocity model in two case studies in North America and found that the 3D velocity model locates events more accurately, especially near the cave boundary. From a tomography perspective, using the 3D velocity model may create a bias in the interpretation since the result of the inversion could also be driven by the initial model. For source location estimates, we can assume that the 3D velocity model derived from borehole-based monitoring is accurate enough to improve the location accuracy compared to the 1D velocity model.

2.1 Ray path tomography

One of the most well-known laws in seismic tomography is Fermat's principle, where the first wave arrival propagates via the faster path which is not necessarily the shortest path in Euclidian distance. In block caving mines, the first-arriving wave should always travel around the cave boundary and not through the cave. The exact path, whether through the yield zone or the seismogenic zone, is unknown. There is no direct investigation that can be used to determine if the first-arrival wave will travel in the yield zone (Figure 1).

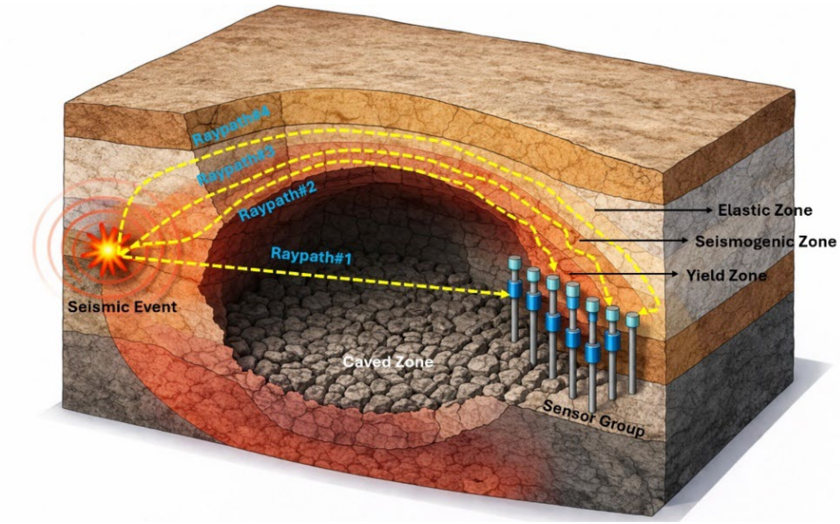

Figure 1 Possible ray path propagation in block caving mines where the seismic event and the sensor group are on opposite sides of the cave. This cave model is based on Sainsbury et al. (2011)

Figure 1 shows how ray paths potentially travel near a cave. Ray path 1 appear impossible since it is not in line with Fermat’s principle. Even if ray path 1 is possible, there will be high attenuation and noise which will make it difficult to identify the first break P-wave arrival. Hence, any available information related to direct cave monitoring instruments should be used in conjunction with the tomographic analysis, similar to well-seismic ties in the oil and gas industry. In this industry, well data are characterised by their high vertical resolutions and are used to tie-in the seismic data to the correct depth. This approach combines detailed vertical information from well logs with the broader horizontal coverage of seismic data, resulting in more precise subsurface imaging.

Figure 2 shows log data being used to calibrate the seismic time to depth conversion. As in active seismic imaging, the depth is converted from the time domain. Well data provide a better understanding of depth and are thus used for the calibration.

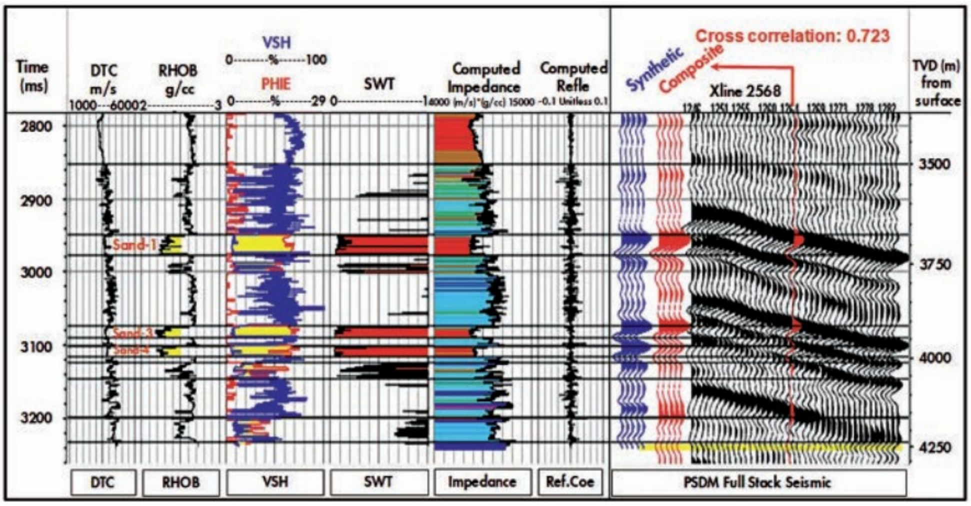

Figure 2 Diagram of well-seismic tie in the oil and gas industry. Well data (left) are used to calibrate the depth of the seismic section (right). Taken from van der Weiden et al. (2012)

This approach is directly applicable to block caving operations, where borehole camera data can be considered analogous to well log measurements due to their superior vertical resolution, whereas seismic tomography provides extensive three-dimensional coverage of the cave region. The integration of these datasets leverages the strengths of both methods, resulting in a more accurate and reliable interpretation of the cave geometry and surrounding rock mass conditions.

2.2 Tomography inversion

This tomographic inversion uses the simultaneous iterative reconstruction technique (SIRT) because it has better convergence and provides smoother results than algebraic reconstruction technique (ART), as described in Crowley et al. (2015).

The 1D velocity model is derived by averaging the travel time plot in the inversion period. The 3D velocity models are derived using estimated cave shapes with very low velocity inside the cave shell and 1D velocity model as the background.

Figure 2 is an artificial-intelligence-generated image that represents the initial 3D velocity model. The model comprises a uniform host rock characterised by solid rock with 4,900 m/s P-wave velocity and a hollow/cave with anomalous very low velocity, 361 m/s for both P-wave and S-wave velocity. The strong velocity contrast between the cave and surrounding rock was introduced to account for the expected seismic response of the cave zone. This initial model serves as the baseline for the inversion.

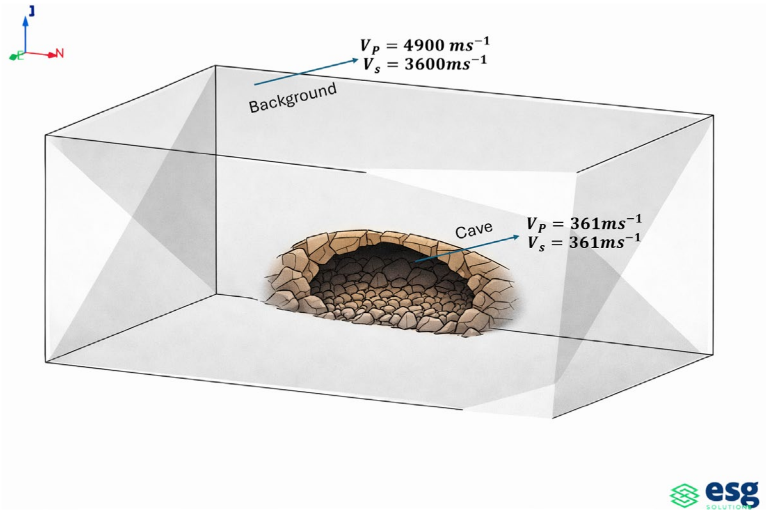

Figure 2 3D velocity model used for the inversion process. The background V_P is an example only and is not used for any actual inversion

Inversion quality control is also performed using a so-called variance matrix. This matrix is calculated for each grid cell based on the inverse Fisher matrix. A Fisher matrix is essentially a quantity that provides a measure of the amount of information that the acquired data contain regarding the parameters that one wishes to estimate from the data (Chao et al. 2016). This quality control is very important because it directly affects the ray coverage, ray density and the resolution.

Passive tomography problems are usually due to the sparse distribution of sensors and uneven events distribution which means it has to deal with the huge, sparse matrices. In this analysis, the inversion is using the improved SIRT with an addition of error estimation and internal parameter constraint that restrict the velocity variation range to predetermined acceptable values.

The run time for an inversion process for ~5,000 events with ~50 sensors and a grid size of 30 × 30 × 30 m is usually 1–2 hours.

3 Tomography analysis

In this study, we use datasets from two different block caving mines. Both mines are in the production stage, are seismically active and have a good sensor distribution for tomographic analysis around the cave. The grid used for the inversion at both sites is 30 × 30 × 30 m.

When plotting the resulting tomography field, only the results with high confidence (low variance) are shown. In both cases, we use 50% as the variance cut-off. The high variance areas are where the ray path density is low or the estimated velocity across different ray paths does not converge, such as in an area where there was no production, meaning that the number of seismic events is also less than in the production zone. While it may still be possible to obtain a tomography image for this area, the variance will be very high because of the lack of ray paths. Near the cave where only limited ray paths are expected to travel (Figure 1), the observed high variance zone may indicate the presence of the cave. However, this interpretation should be made carefully. To test this interpretation, another data source, such as mucking or any direct borehole-based measurements, must be used.

The legend for each tomography section is 4,000 ms^{-1} to 6,500 ms^{-1} as shown in Figure 3.

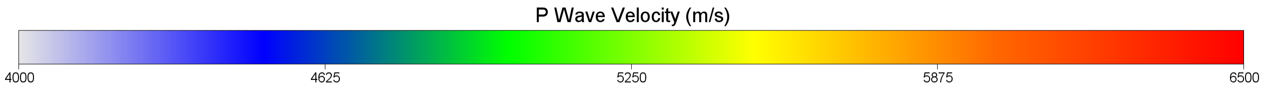

Figure 3 Legend for tomography sections

3.1 Cave A

Cave A, depicted in Figure 4, is located hundreds of metres below the surface with an open pit/subsidence area located above the cave. Production is occurring on the right-hand side of the cave and is the area of highest seismicity. Tomography results from three consecutive 1-week periods are compared in Figures 5 and 6. While the transparent views appear to show seismic events inside the cave, this effect is caused by the viewing angle.

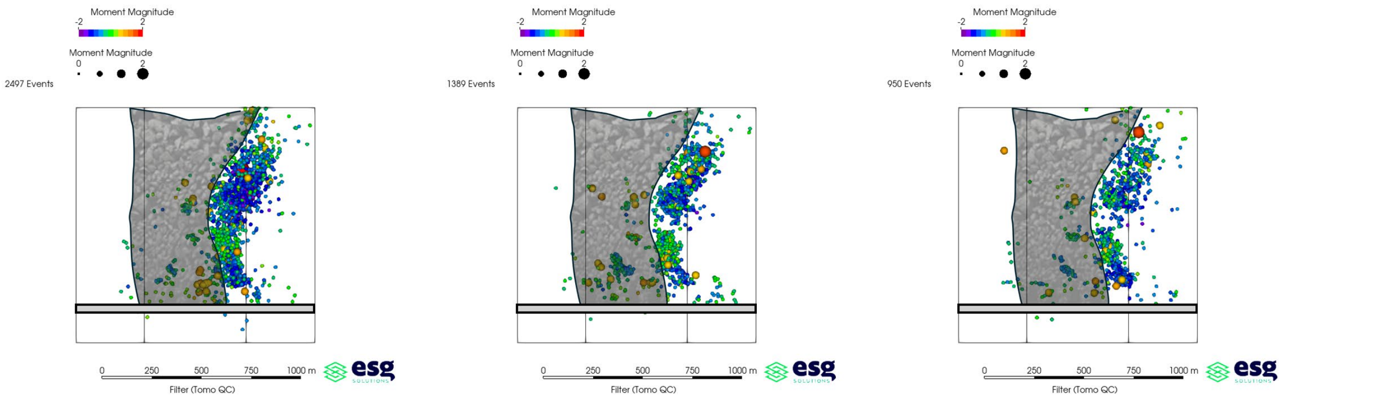

(a) (b) (c)

Figure 4 Weekly seismic distribution used in the inversion process. (a) Week 1; (b) Week 2; (c) Week 3

Figure 4 shows that the first week was the most seismically active, followed by the second and third weeks. This was because during the second week, there was a maintenance period where all mining activities stopped. Production recommenced in Week 3, but with only small tonnages compared with Week 1. Figure 4 also shows that there is seismicity only on the right-hand side of the cave where production blasting is occurring. This side of the cave is the area of interest for tomography inversion.

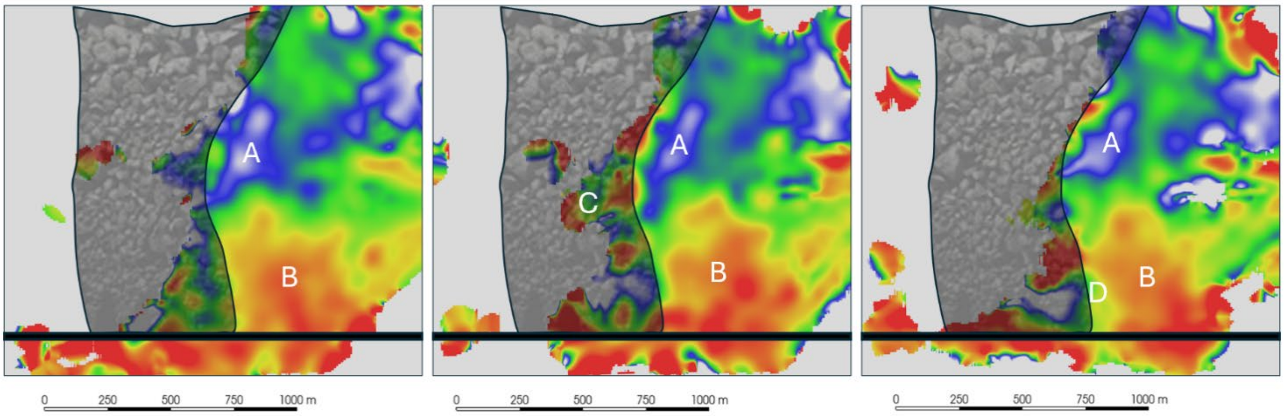

(a) (b) (c)

Figure 5 Tomography section view results from inversion with a 1D velocity model. A local polynomial smoothing was applied to suppress artefacts. (a) Week 1; (b) Week 2; (c) Week 3. The grey zone shows where tomography inversion results are of low confidence

Figure 5 shows the tomography results using the 1D velocity model as the starting velocity estimate. The grey zone is a predetermined estimate of the cave shape obtained from other methods. Most of the area inside the estimated cave location has low-confidence tomography results, indicating low ray path coverage. In all three periods, the inversion result shows a low velocity zone to the left of the neck of the cave (marked as A) and relatively high velocity in the abutment (marked as B). The area below the cave shows high P-wave velocity for all three weeks of the analysis.

In Week 2 (middle image), there is a mix of high and low velocity zones located inside the neck of the estimated cave location (marked as C), which is not present in Week 1 (left-hand side image). This velocity information located inside the estimated cave shape suggests wave propagation inside the cave estimate. This may indicate that the rock in these areas is not as fractured as previously thought and the cave is not as advanced as the estimated cave shape. This may also be a gridding artefact or an error associated with a reduction of ray paths (that is still below the maximum variance threshold) towards the edge of the usable field. Alternatively, it could be a gridding effect, or the inversion might be plausible, suggesting that seismic waves are propagating through the yield zone; this implies that these regions can still transmit seismic energy or that this zone has not actually caved yet. Without direct borehole measurements in this area, it is not possible to determine if there is still some intact rock. The seismogenic zone does show where there is sufficiently intact rock that is capable of producing seismicity. Comparing Figures 4 and 5, the low velocity zone A corresponds to a seismically active area, indicating that the rock in this area has not yet failed.

In Week 3 (right-hand side image), the tomography section no longer shows the high/low velocity areas inside the estimated cave shape, which may indicate that the mucking has relieved this zone because the removal of the caved zone creates a clear contrast between a hollow cave and the abutment. In addition, near the abutment of the cave line at low elevation (marked as D), a lower velocity profile is detected, indicating that the stress is moving in the direction of production.

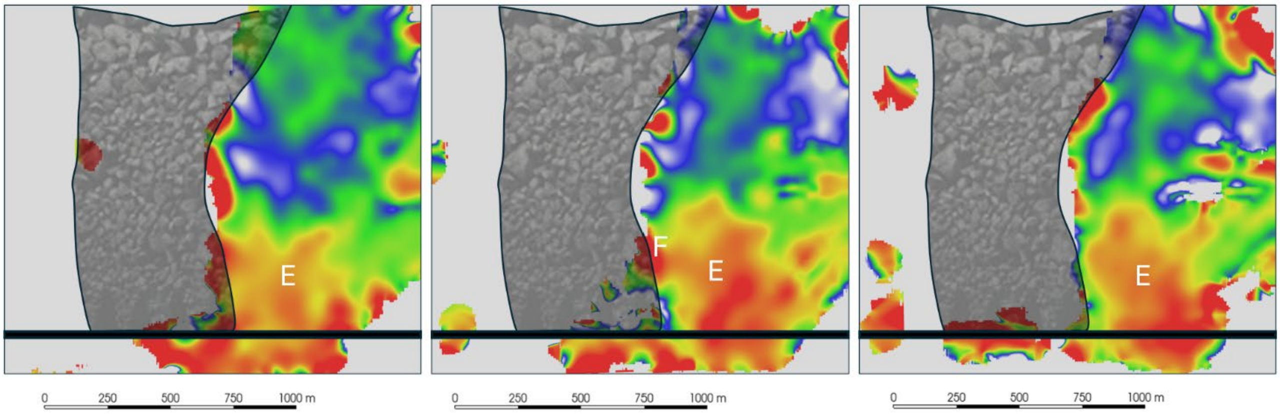

(a) (b) (c)

Figure 6 Tomography section view result from inversion using 3D velocity model (estimated cave shape used as constraint). (a) Week 1; (b) Week 2; (c) Week 3. Grey zone shows where tomography inversion results are of low confidence

Figure 6 shows the inversion results obtained from using a 3D velocity model as the starting estimate. These results show the same trends in velocity that are observed in the results obtained from using the 1D velocity model as the starting estimate (Figure 5). The abutment is dominated by a high velocity profile (marked as E) and a low velocity area is located to the right of the cave neck.

In the middle image of Figure 6, the abutment shows an increase in P-wave velocity compared to the previous week. In Week 3 (right-hand side image), a higher velocity zone is observed further to the right and more in line with the extraction level. This condition may be driven by the restart o mucking and production. The nearby abutment (middle image, marked as F) also shows a high modelled velocity profile. Both inversion results show a high velocity profile below the cave/below the production zone.

3.2 Cave B

Cave B is in a similar environment as Cave A, located hundreds of metres below the surface, but is seismically active on both sides of the cave. However, Cave B is smaller than Cave A. Unlike Cave A where seismic activity is mainly concentrated near mucking and blasting, Cave B shows relatively active seismicity throughout the entire cave, even though undercutting advances only on the right-hand side.

For this investigation, we look at three consecutive months during active production. In the first month, intense mucking was performed in all drawpoints below the cave. In the second and the third months, the production was significantly decreased and mucking only occurred on the right-hand side of the cave. This is evident from the decreasing of seismic activity from the first to third month.

Figure 7 shows the seismicity distribution in Cave B. The figure shows that there was a low cluster of seismic activity in the area above the estimated cave shape, which become lesser from Month 1 until Month 3. However, in the abutment (right-hand side of the cave) and every corner of the estimated cave, the seismic activity is relatively stable. Sensor distribution in Cave B is very good; sensors exist in almost all directions from the cave. This situation created good coverage in terms of ray path density. While the transparent views appear to show seismic events inside the cave, this effect is caused by the viewing angle.

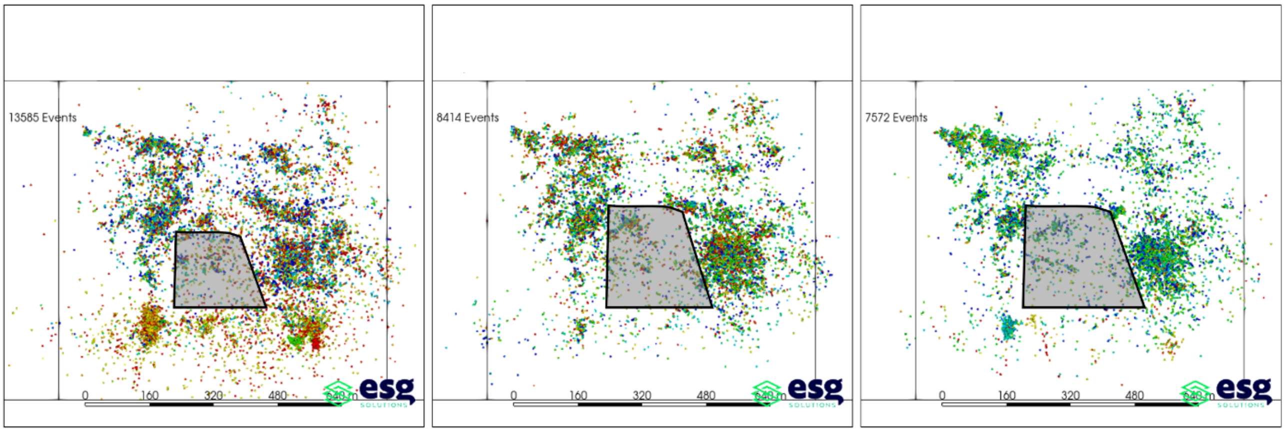

(a) (b) (c)

Figure 7 Seismic distribution across three months for the inversion process. (a) Month 1; (b) Month 2; (c) Month 3

The cave growth was estimated using the HOD approach, which suggests that cave growth or cave advance was concentrated in the zones of ongoing mucking activities. In the first month (left-hand side image), the cave is relatively small and seismic activity appear to exist above the left-hand and right-hand sides of the cave. Meanwhile from Month 2 to Month 3, the estimated cave did not grow; it only expanded to the right-hand side. From a seismicity point of view, the cluster above the cave in months 2 and 3 has disappeared. The cluster on the right-hand side (abutment) moved to the right between months 2 and 3. Figure 8 shows the inversion result of this dataset.

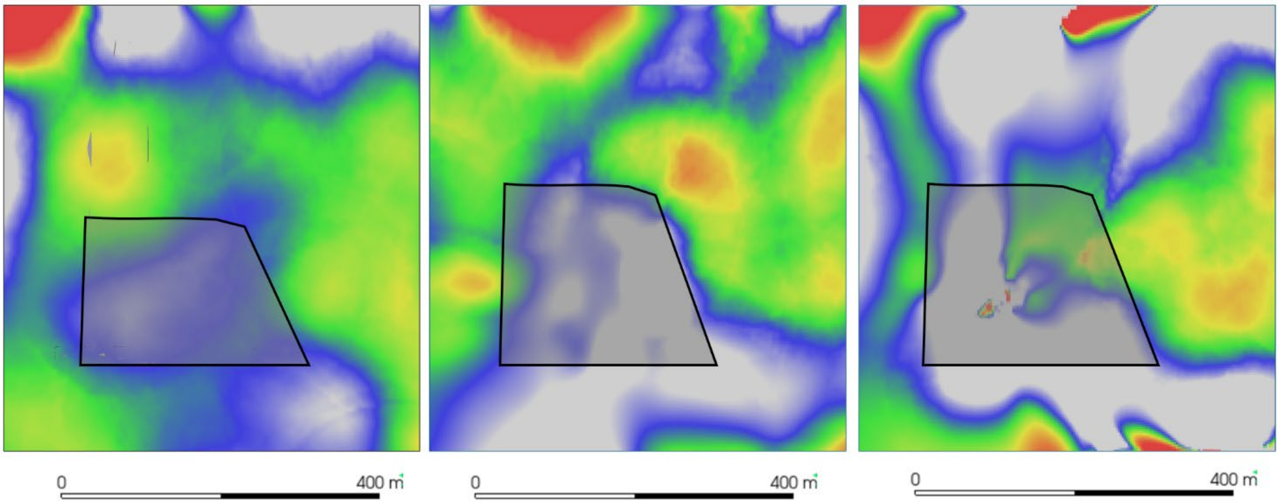

(a) (b) (c)

Figure 8 Tomography section view results from inversion without 3D velocity model. (a) Months 1; (b) Month 2; (c) Month 3. The grey zone inside the trapezium line is the estimated cave based on the HOD

The result of inversion without a 3D velocity model indicates that the velocity profile is still well constrained with the estimated cave. In the first month, the area inside the estimated cave shows low velocities. In the second and third months, it appears predominantly grey, indicating insufficient ray path coverage or confidence. For comparison, the result of inversion using the 3D velocity model is shown in Figure 9.

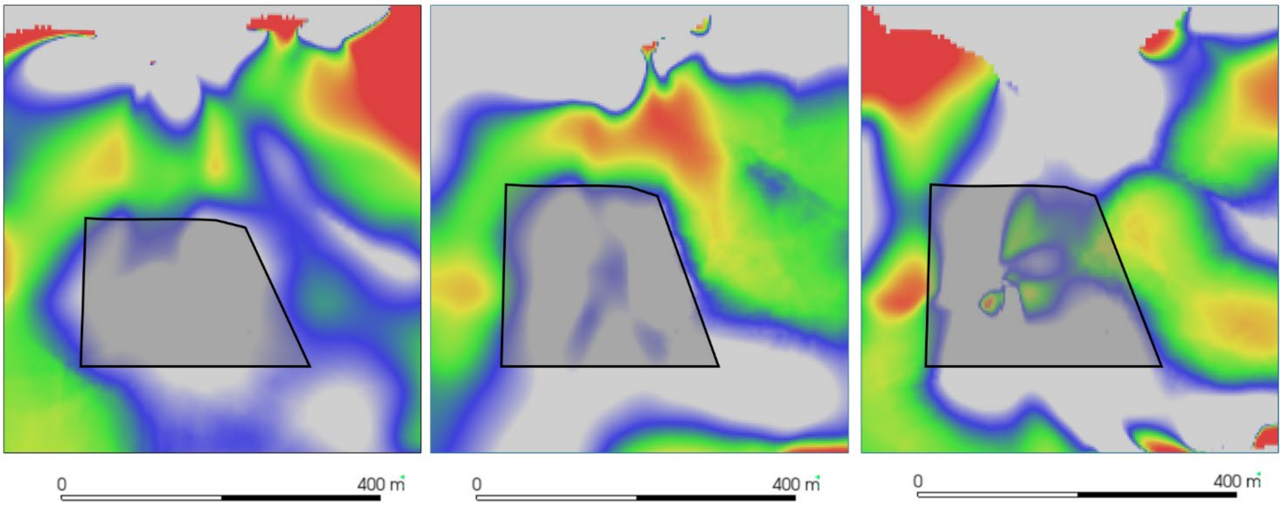

Figure 9 Tomography section view results from inversion using a 3D velocity model. (a) Months 1; (b) Month 2; (c) Month 3. Grey zone is where tomography has low-confidence inversion results

In the first month of datasets, Figure 7 and Figure 8 (left) show that the grey area is larger in the inversion using the 3D velocity model. As a result, in the left-hand side of the cave, the tomography section using a 3D velocity model (Figure 1) created a grey zone which could be interpreted as the cave extending in this direction, but the production data showed that advance undercutting was not towards this direction. The result of inversion without the 3D velocity model shows more confidence in the result as the low velocity zone is well constrained with the estimated cave (no grey area in the left abutment). This also happened in the top right-hand side, but looking at the advance undercutting direction, this could have been influenced by mucking and actual cave propagation.

In Month 2, the left-hand side of the cave shows an increase in the P-wave velocity estimate at the abutment. This makes sense as the cave is growing in height, putting more stress on the abutments. The 1D and 3D tomography results both show the growth at the top of the cave between months 1 and 2. The growth there is most likely transferring the stress towards the lower elevation. Since it cannot be transferred inside the cave, the stress moves to the abutment. An increase in P-wave velocity is detected in the lower abutment in the following months.

In Month 3, the tomography results show very similar patterns: both results show a grey zone above the cave, which might be indicative of significant cave growth. This observation is supported by the increase in the P-wave velocity model in the left-hand side, top right and the bottom right (abutment), which is most probably the result of stress transfer due to the cave growth. However, both inversions also show P-wave velocity estimates inside the estimated cave shape. This indicates that some ray paths are still allowed to propagate through this zone, raising the question of whether this zone is a cave or muck pile that remains sufficiently competent to be passed by ray paths.

4 Discussion

Tomography is based on the ray paths, and ray paths should be allowed to be modelled freely without an initial cave model which forces them to propagate outside that estimated cave shape. From this case study the 1D and 3D starting velocity models are both capable of capturing the observed cave growth. While each approach is subject to its own constraint regarding the cave geometry, both approached provide valuable insight in the evolution of the caved zones. In the practice of mine seismology, the two methods should be used together, not just the 3D cave constraint but also the 1D without cave constraint.

In some block caving settings, direct measurements of the 3D cave shape can be made, but in other settings this is not feasible. The borehole and tomography should be used together, similar to well-seismic ties in the oil and gas industry where active seismic imaging is not driven by 3D well log interpolation but instead complements and is constrained by the borehole information.

5 Conclusion

This study demonstrates that the use of a predefined 3D velocity model in seismic tomography can introduce bias by constraining inversion results towards estimated cave geometry, potentially masking true subsurface conditions. In contrast, unconstrained inversion allows ray paths to be governed more freely by observed travel time data, revealing alternative structures that may better represent the actual state of the rock mass. Therefore, a combined approach of inversion using both 1D and 3D velocity models is recommended to achieve a more balanced and reliable interpretation of cave shape and stress evolution in block caving environments.

However, this work requires further study. We suggest that in the future, comparing tomography from different source location delineation, delineation with cave and without cave constraint, and comparing the results against any available borehole-based measurements and production data will likely deliver a better understanding of how the cave evolves.

Acknowledgement

The author wishes thanks to Doug Angus, Sebastian Braganza and Dave Collins (ESG Solutions, Canada) for detailed internal review and suggestions.

References

Afrouz, S & Westman, E 2018, 'Review and simulation of passive seismic tomography in block cave mining', in Y Potvin & J Jakubec (eds), *Caving 2018*, Australian Centre for Geomechanics, Perth, pp. 223–230, https://doi.org/10.36487/ACG_rep/1815_14_Afrouz

Chao, J, Ward, ES & Ober, RJ 2016, 'Fisher information theory for parameter estimation in single molecule microscopy: tutorial', *Journal of the Optical Society of America*, vol. 33, no. 7, pp. B36–B57.

Crowley, J, Baig, A & Urbancic, T 2015, '4D tomography and deformation from microseismic data', *85th Annual Meeting of the Society of Exploration Geophysics*, Society of Exploration Geophysicists, Tulsa.

Collins, D, Toya, Y, Pinnock, I, Shumila, V & Hosseini, Z 2014, '3D velocity model with complex geology and void for Microseismic location and mechanism', in M Hudyma & Y Potvin (eds), *Deep Mining 2014*, Australian Centre for Geomechanics, Perth, pp. 681–689, https://papers.acg.uwa.edu.au/p/1410_48_Collins/

Dawn, T 2019, 'Technologies of ground support monitoring in block caving operations', in J Hadjigeorgiou & M Hudyma (eds), *Ground Support 2019: Proceedings of the Ninth International Symposium on Ground Support in Mining and Underground Construction*, Australian Centre for Geomechanics, Perth, pp. 109–122, https://papers.acg.uwa.edu.au/p/1925_06_Dawn/

de Beer, W, William, R, Prahastudhi, S & Braim, M 2024, 'Advanced analysis of seismic data to validate critical assumptions', in P Andrieux & D Cumming-Potvin (eds), *Deep Mining 2024: Proceedings of the 10th International Conference on Deep and High Stress Mining*, Australian Centre for Geomechanics, Perth, pp. 981–994, https://doi.org/10.36487/ACG_repo/2465_62

Grand, SP, van der Hilst, RD & Widiyantoro, S 1997, 'Global seismic tomography: a snapshot of convection in the Earth', *GSA Today*, vol. 7, no. 4, pp. 1–7.

Setiadi, H, Bagus, BEB, Nurhandoko, Wely, W, Riyanto, E 2015, 'Prediction of subsurface fracture in mining zone of Papua using passive seismic tomography based on Fresnel zone', *The 5th Asian Physics Symposium*, AIP Publishing, https://doi.org/10.1063/1.4917152

Kamp, C, Conley, A, Collins, DS, Preiksaitis, M, Butler, T & Shumila, V 2022, 'Use of seismic tomography to aid rock mechanics interpretation at New Afton B3 block cave mine', in Y Potvin (ed.), *Caving 2022: Proceedings of the Fifth International Conference on Block and Sublevel Caving*, Australian Centre for Geomechanics, Perth, pp. 461–472, https://doi.org/10.36487/ACG_repo/2205_31

Melati, S, Wattimena, R, Sahara, D, Simangunsong, G, Wibowo, A, Hidayat, W & Riyanto, E 2025, 'Modelling cave propagation in deep block caving by incorporating the fracture zone inferred from seismic tomography', *Mining of Mineral Deposits*, vol. 19, no. 87–97, http://mining.in.ua/2025vol19_3_9.html

Muttaqy, F, Nugraha, AD, Mori, J, Puspito, NT, Supendi, P & Rohadi, S 2022, 'Seismic imaging of lithospheric structure beneath Central-East Java Region, Indonesia: relation to recent earthquakes', *Frontiers in Earth Science*, vol. 10, article 756806, http://dx.doi.org/10.3389/feart.2022.756806

Rahman, A, Fransisco, L & Wahyudi, W 2013, 'Application of passive seismic to minimize subsurface uncertainties in exploration, a case history of Selong and Akatara prospect, Jambi sub-basin'*, HAGI-IAGI Joint Convention 2013*.

Sainsbury, BL & Sainsbury, DP & Pierce, ME 2011, 'A historical review of the development of numerical cave propagation simulations', *Proceedings of the 2nd International FLAC/DEM Symposium*, ITASCA Consulting Group.

van der Weiden, R, Nayak, P & Swinburn, P 2012, 'Seismic technology supporting reserves determinations: Gorgon Field, Australia', *The Leading Edge*, vol. 31, no. 9, pp. 1050–1057.